ACS APPLIED MATERIALS & INTERFACES

www.acsami.org

Research Article

Gas-Permeable Inorganic Shell Improves the Coking Stability and Electrochemical Reactivity of Pt toward Methane Oxidation

Jongsu Seo, Nikolai Tsvetkov, Seung Jin Jeong, Yeongeun Yoo, Sanghoon Ji, Jeong Hwan Kim,* Jeung Ku Kang,* and WooChul Jung*

Cite This: *ACS Appl. Mater. Interfaces* 2020, 12, 4405−4413

Read Online

ACCESS | Metrics & More | Article Recommendations | Supporting Information

ABSTRACT: Solid oxide fuel cells produce electricity directly by oxidizing methane, which is the most attractive natural gas fuel, and metal nanocatalysts are a promising means of overcoming the poor catalytic activity of conventional ceramic electrodes. However, the lack of thermal and chemical stability of nanocatalysts is a major bottleneck in the effort to ensure the lifetime of metal-decorated electrodes for methane oxidation. Here, for the first time, this issue is addressed by encapsulating metal nanoparticles with gas-permeable inorganic shells. Pt particles approximately 10 nm in size are dispersed on the surface of a porous $La_{0.75}Sr_{0.25}Cr_{0.5}Mn_{0.5}O_3$ (LSCM) electrode via wet infiltration and are then coated with an ultrathin Al_2O_3 layer via atomic layer deposition. The Al_2O_3 overcoat, despite being an insulator, significantly enhances the immunity to carbon coking and provides high activity for the electrochemical oxidation of methane, thereby reducing the reaction impedance of the Pt-decorated electrode by more than 2 orders of magnitude and making the electrode activity of the Pt-decorated sample at 650 °C comparable with those reported at 800 °C for pristine LSCM electrodes. These observations provide a new perspective on strategies to lower the operation temperature, which has long been a challenge related to hydrocarbon-fueled solid oxide fuel cells.

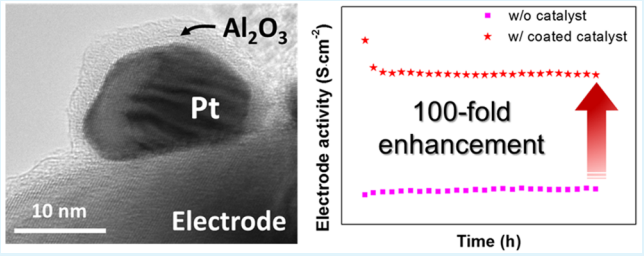

KEYWORDS: *solid oxide fuel cell, metal nanocatalyst, atomic layer deposition, ceramic anode, direct methane*

INTRODUCTION

A fuel cell is an electrochemical device that converts the chemical energy of a fuel into electrical energy through electrochemical reactions. While hydrogen is the highest energy carrier, its utilization still raises many technical issues related to production, storage, and transportation. In this regard, solid oxide fuel cells (SOFCs), which can directly use hydrocarbon fuels, are highly promising devices for commercialization, with the goal of their use in small and large-scale applications.[1] However, state-of-the-art SOFC anodes, which are typically composed of nickel and yttria-stabilized zirconia (YSZ) with the former serving as an electronically conducting electrocatalyst and the latter providing an oxygen ion transport pathway, are unsuitable for hydrocarbon electro-oxidation owing to Ni-catalyzed carbon deposition, which severely degrades the anode performance.[1,2]

As an alternative to nickel/YSZ cermet, other conducting oxide materials such as $(La,Sr)(Cr,Mn)O_3$, $(La,Sr)TiO_3$, $PrBaMn_2O_5$, and $(Sm,Ce)O_2$ have been actively studied because of their thermomechanical and chemical stability.[2−8] Among them, LSCM is known to have excellent resistance to carbon deposition and good stability in both oxidative and reductive environments as well as sufficiently high mixed ionic and electronic conductivity.[9−11] Meanwhile, the catalytic activity of these ceramic anodes for methane oxidation is not sufficient at intermediate temperatures (500−700 °C),[12] necessitating an increase in the operation temperature. However, this increases the device cost and decreases the lifetime.

Related to this, metal nanoparticles (NPs) have excellent catalytic activity and have been studied extensively in the area of heterogeneous catalysis.[13,14] On the other hand, the tendency to agglomerate because of the poor thermal and chemical stabilities of nanosized particles is a stumbling block preventing their utilization in high-temperature applications including SOFCs. Over the past few decades, there have been many attempts to develop thermally robust metal catalysts, and successful physical protection strategies to encapsulate metal NPs with robust inorganic shells have been reported in recent years.[15] In these cases, it is crucial to design the morphology and structure of the shell accurately, as different shell layers of catalysts result in very different catalytic activities.[15−18] Accordingly, precise control of the thickness and uniformity of the shell layer is of primary importance when attempting to

Received: September 10, 2019
Accepted: December 31, 2019
Published: December 31, 2019

https://dx.doi.org/10.1021/acsami.9b16410
ACS Appl. Mater. Interfaces 2020, 12, 4405−4413

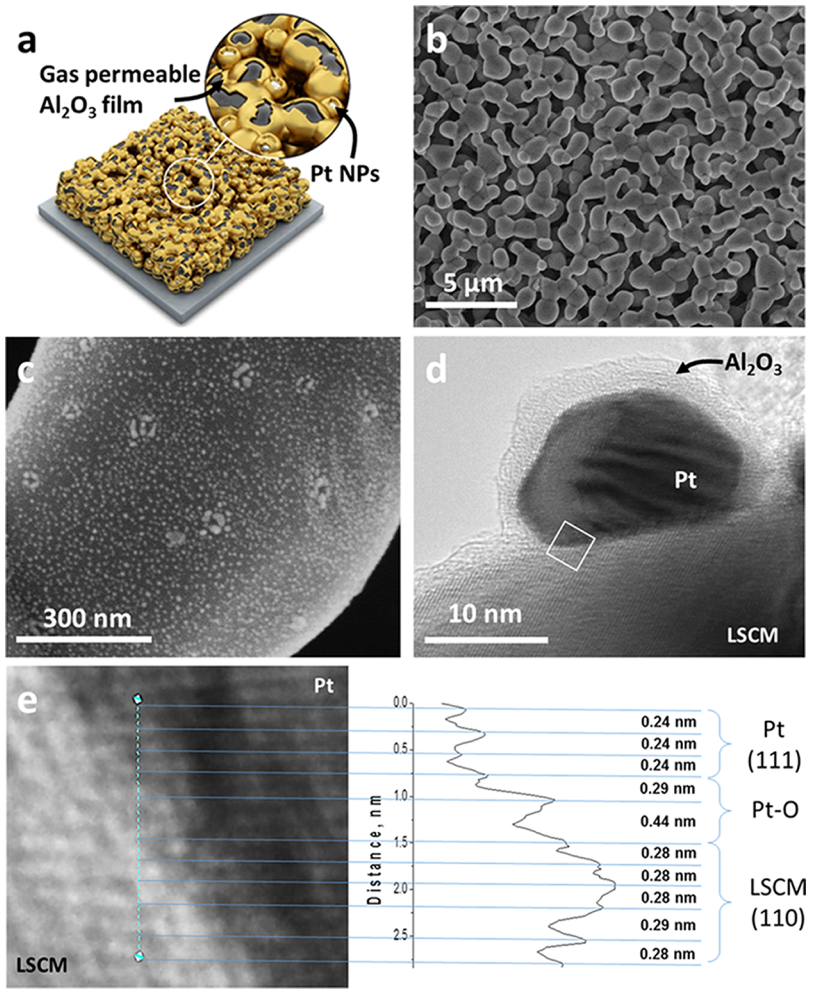

Figure 1. Microscopic images of Pt-decorated $La_{0.75}Sr_{0.25}Cr_{0.5}Mn_{0.5}O_3$ with Al_2O_3 coating. (a) Schematic image of a fabricated electrode. The SEM images of (b) pristine $La_{0.75}Sr_{0.25}Cr_{0.5}Mn_{0.5}O_3$ and (c) Pt-infiltrated $La_{0.75}Sr_{0.25}Cr_{0.5}Mn_{0.5}O_3$. (d) TEM image of a Pt NP on $La_{0.75}Sr_{0.25}Cr_{0.5}Mn_{0.5}O_3$ support covered with the Al_2O_3 layer and (e) magnified image for the inside of the square at (d) and the TEM signal intensity along the blue dotted line, where the peaks correspond to the positions of the atoms at the lattice fringes.

improve catalyst performance capabilities. Further, the shell needs to be formed at a sufficiently low temperature such that the particles do not become aggregated. Atomic layer deposition (ALD) can be used to meet these requirements for control of the deposition layers on the atomic scale without high-temperature annealing, highlighting its potential to realize thermal and chemical stability of nanocatalysts. Recently, numerous reports have shown that an ALD overcoat greatly improves the high-temperature durability of metal NPs. Meanwhile, it is worth noting that most of the studies reported in the literature on the stabilization of metal NPs using ALD focus more on chemical heterogeneous catalysts or fuel cells operated at low temperatures.[19−28] Only a few studies can be found on the application of ALD to SOFCs. ALD coatings have been used to prevent the decomposition of electrode materials,[29−35] to fabricate electrolyte layers,[36−40] or to modulate electrode surface properties.[41,42] However, to the best of our knowledge, there is no report on stabilizing metal NPs dispersed on an electrode surface through ALD in relation to high-temperature electrochemical catalysis (Tables S1 and S2). It is notable that although researchers have focused on chemical catalysts, some have successfully stabilized metal nanocatalysts under operating conditions similar to those of SOFC fuel-electrodes. For example, Al_2O_3-encapsulated Pd NPs were reported to show excellent catalytic activity for the oxidative dehydrogenation of ethane at 675 °C for 28 h with high thermal and chemical stability levels via a trade-off between the stability and catalyst activity depending on the coating thickness.[43] These earlier results suggest that similar strategies can be applied to high-temperature ceramic-based fuel cells if current collection or gas flux issues are properly considered.

In this study, for the first time, we show that an ultrathin Al_2O_3 (alumina) overcoating of supported Pt NPs can effectively reduce carbon coking and catalyst particle agglomeration, thus enabling the realization of highly reactive SOFC electrodes. As a case study, we select $La_{0.75}Sr_{0.25}Cr_{0.5}Mn_{0.5}O_3$ (LSCM) as a mixed conducting electrode material and distribute monodisperse Pt NPs with a diameter of ∼10 nm on its surface. Al_2O_3 films with thicknesses of several nanometers are then deposited onto the surface via ALD at a temperature of 200 °C using trimethylaluminum ($C_6H_{18}Al_2$) and water as an Al precursor and oxidant, respectively. The physical and chemical attributes of each coated electrode are characterized by a range of analysis tools including ellipsometry, scanning electron microscopy (SEM), transmission electron microscopy (TEM), and in situ X-ray photoelectron spectroscopy (XPS).

https://dx.doi.org/10.1021/acsami.9b16410
ACS Appl. Mater. Interfaces 2020, 12, 4405−4413

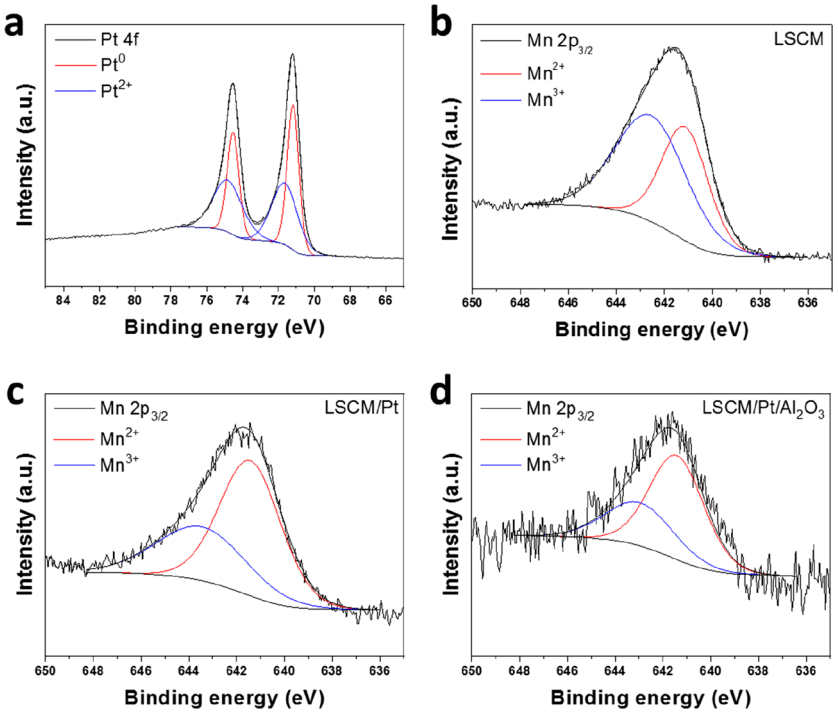

Figure 2. In situ XPS analysis. The deconvolution of (a) the Pt 4f core-level peak spectrum recorded from bare Pt sample and the Mn 2p core-level peak spectra recorded from (b) pristine LSCM, (c) bare Pt, and (d) Pt/Al_2O_3 samples.

Electrical conductivity relaxation measurements[44] are also conducted to estimate the surface coverage of Al_2O_3 films with different thicknesses on LSCM electrodes. Finally, an analysis by electrochemical impedance spectroscopy (EIS) of bare LSCM, Pt/LSCM, and Al_2O_3/Pt/LSCM electrodes for methane oxidation reveals that Pt NPs encapsulated in Al_2O_3 show improved electrode activity by more than 100 times. Moreover, the activity values achieved at 650 °C in our work are comparable to those of an LSCM anode at 800 °C.[45] Thus, the developed approach of electrode decoration with encapsulated metal NPs enables one to decrease the operation temperature of a SOFC anode by more than a hundred degrees without sacrificing the performance.

RESULTS AND DISCUSSION

Figure 1a shows the concept of a SOFC anode decorated with the catalysts used in this study. Pt NPs approximately 10 nm in size were uniformly deposited using a wet-infiltration method onto the surface of a porous LSCM electrode, which was prepared by screen-printing and subsequent sintering onto an YSZ substrate (Figure 1b,c). Al_2O_3 layers with thicknesses ranging from 1.0 to 3.0 nm were then deposited onto the Pt-decorated LSCM surface using ALD. Hereafter, we refer to the LSCM sample decorated with Pt as the "bare Pt" sample, with the sample on which Al_2O_3 is additionally coated referred to as the "Al_2O_3/Pt" sample. TEM measurements confirm that the 2.0 nm thick Al_2O_3 layer covers the surfaces of the LSCM and Pt NPs uniformly (Figure 1d). The corresponding elemental maps for La, Pt, and Al are shown in Figure S1. It should be noted that the Al_2O_3 was deposited at a constant growth rate regardless of the precursor pursing time, indicative of uniform layer-by-layer growth (Figure S2).

A TEM analysis was conducted to investigate the interface between the Pt NPs and LSCM support in detail. The change in the interplanar distance across the LSCM/Pt interface was determined by monitoring the evolution of the TEM signal across the interface (Figure 1e), where the peaks in the spectrum correspond to the positions of the cations in the lattice fringes such that the distance between the peaks reflects the interplanar distance between the ALDs. Within the Pt particle, the interplanar distance is around 0.24 nm, close to that of Pt(111). On the other hand, within the LSCM particle, the measured distance of approximately 0.28−0.29 nm is found to be in agreement with that of the LSCM(110) lattice spacing. However, at the interface, we observed significantly enlarged lattice distances up to approximately 0.29−0.44 nm, which are attributed to the formation of long Pt−O−Pt bonds within the PtO interface layer.[46]

We also analyzed the chemical nature of Pt-decorated LSCMs with and without Al_2O_3 coating through XPS measurements. A bare LSCM sample exhibits only peaks related to La, Sr, Co, and Mn cations without any impurity species (Figure S3). The quantitative analysis revealed that the (La + Sr)/(Co + Mn) and La/Sr ratios are close to stoichiometric ratios of 1/1 and 3/1, respectively. After the deposition of Pt and Al_2O_3, Pt and Al peaks were observed in the spectra, but the (La + Sr)/(Co + Mn) and La/Sr ratios remained identical to those in the bare LSCM sample. In addition, for a more in-depth evaluation of the effects of Pt and Al_2O_3 depositions on the oxidation states of the transition metals and Pt, in situ XPS measurements were taken under conditions close to the actual highly reducing electrode operation conditions, that is, a temperature of 650 °C and an ultrahigh vacuum atmosphere. Here, the sample was heated at 650 °C inside the analysis chamber in XPS. We find that the Pt 4f core-level peaks for the LSCM/Pt sample have two features corresponding to metallic Pt^0 and oxidized Pt^{2+} (Figure 2a).[47] It is notable that in the ultrahigh vacuum (UHV) conditions used for the in situ XPS measurements, the complete reduction of Pt oxides readily takes place at

https://dx.doi.org/10.1021/acsami.9b16410
ACS Appl. Mater. Interfaces 2020, 12, 4405−4413

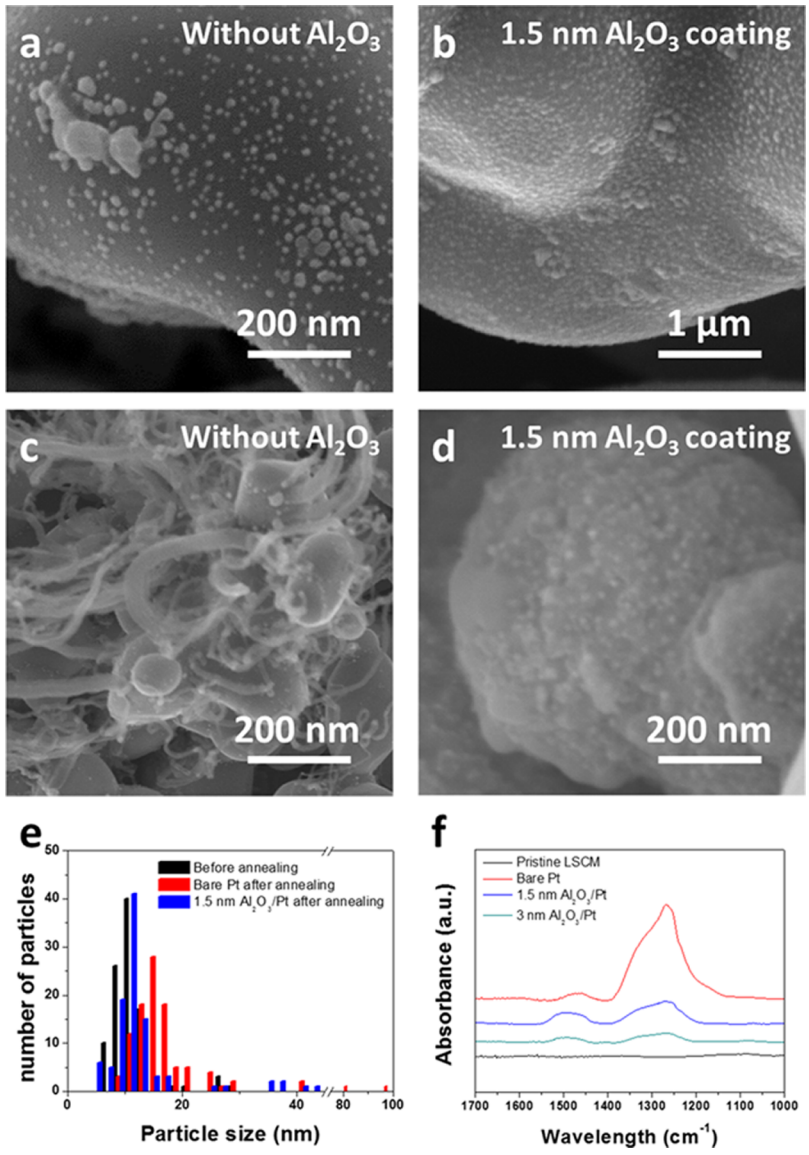

Figure 3. Sintering and coking resistance of the Al_2O_3-decorated Pt NPs. SEM images of Pt-decorated $La_{0.75}Sr_{0.25}Cr_{0.5}Mn_{0.5}O_3$ (a) without and (b) with Al_2O_3 coating after sintering at 700 °C for 1 h in air. The SEM images of Pt-decorated $La_{0.75}Sr_{0.25}Cr_{0.5}Mn_{0.5}O_3$ (c) without and (d) with Al_2O_3 coating after carbon coking at 650 °C for 25 h under wet (2% H_2O) CH_4. (e) Corresponding size distribution of Pt NPs after sintering at 700 °C and (f) corresponding FTIR absorption spectra of the electrodes after carbon coking at 650 °C under wet CH_4.

temperatures below 200 °C.[48] Interestingly, however, quantitative analyses demonstrate that with the LSCM support, nearly half of the Pt is still oxidized even at 650 °C. The observation of the oxidized Pt state at such a high temperature indicates that electron and/or oxygen ion transfer between Pt NPs and the LSCM support are taking place, thereby modifying the electronic structure of the interface between the LSCM and Pt. It should be noted that the supporting oxide can change the electronic structure of Pt in the 5d valence band orbital of Pt by transferring an oxygen ion, leading to the formation of the observed Pt^{2+}.[49] At the same time, a stable Pt monoxide layer can form at the interface because of metal−support interaction when the excess interface formation energy stabilizes the Pt oxide against dissociation.[46] This is in good agreement with the enlargement of the lattice spacing observed in the TEM analysis here (Figure 1e), and we can propose that a thin PtO layer exists at the interface between the Pt NPs and LSCM, even under significant reducing conditions.

Moreover, the presence of the Pt NPs causes a significant change in the Mn-oxidation state, implying charge transfer between the Pt NPs and the ceramic support. The Mn 2p core-level peak spectra for different samples are shown in Figure 2a−c. For the bare LSCM, two distinguishable features corresponding to Mn^{2+} and Mn^{3+} oxidation states with a more intense Mn^{3+} peak were observed.[50] Quantitative analyses show that the Mn^{2+}/Mn^{3+} ratio is approximately 4/6, indicating that the Mn oxidation state is close to +2.6. On the other hand, Pt deposition leads to a reduction of Mn to the +2.4 oxidation state. In contrast, we do not observe any significant change in the Cr oxidation state upon the deposition of Pt or Al_2O_3 (Figure S4).

It is well known that Pt catalyzes the absorption and dissociation of methane (CH_4). Accordingly, the surfaces of Pt nanocatalysts can be predicted to serve as key reaction sites for

https://dx.doi.org/10.1021/acsami.9b16410
ACS Appl. Mater. Interfaces 2020, 12, 4405−4413

methane electrochemical oxidation or steam reforming, which are possible SOFC anode reactions. Furthermore, the observed PtO interlayer suggests the partial reduction of Mn around the Pt particles and hence the formation of oxygen vacancies. The increased concentration of oxygen vacancies around the reduced Mn sites can have a positive effect on the reactivity of the anode.[51] In addition to these aspects, the oxidized Pt cluster itself can significantly affect the catalytic activity by serving as a barrier-free active site for gas absorption.[52] Therefore, as will be discussed below, the improvement of the electrode activity is attributed to the combined effect of the metal−support interaction between the LSCM and Pt as well as the excellent catalytic activity of Pt particles. A detailed role of the interplay between LSCM and Pt deserves further investigation.

In contrast to the Pt particles, the Al_2O_3 layer does not affect the electronic structure of LSCM (Figure 2c,d). The EIS analysis also confirms that the Al_2O_3 coating does not show catalytic activity for H_2 oxidation (Figure S5). Based on these results, we can conclude that Al_2O_3 films physically protect the surface morphology rather than altering the electronic structure and related chemical reaction pathways; moreover, the Al_2O_3 overcoat is expected to passivate only the reaction sites on the LSCM surface, as Al_2O_3 is not reactive. Accordingly, the ultrathin Al_2O_3 layer must partially cover the electrode surface, not completely, so that CH_4 gas can be sufficiently supplied. In this study, we have quantitatively analyzed the LSCM surface coverage of the Al_2O_3 overcoat by measuring the surface reaction rates (see Section S8 for a detailed analysis). It was found that the coverage was determined to change from 60% for the 1.0 nm thick Al_2O_3 film to 93% for the 3.0 nm thick film, confirming that the ALD layer does not completely passivate the electrode surface. The incomplete coverage of the LSCM surface with the Al_2O_3 layer even with the 3.0 nm thick film can be explained by the fact that the ALD layer heat-treated at 650 °C is porous and permeable to gases owing to the removal of residual carbon species and Ostwald ripening at high temperatures.[43]

We also investigated whether a coating layer with a nanoscale thickness can stabilize Pt particles sufficiently at high temperatures and in CH_4 atmospheres. The morphologies of the Pt particles dispersed on the LSCM electrode are proven to change depending on the presence (Figure 3a) or absence (Figure 3b) of the Al_2O_3 overcoat after annealing in air at 700 °C for 1 h. Bare Pt particles agglomerate readily at this temperature, and the 1 nm thick Al_2O_3 overcoat (Figure S8a) does not effectively inhibit the aggregation of individual particles, whereas it prevents the formation of Pt clusters of several hundred nanometers. In contrast, those coated with an Al_2O_3 layer having a thickness of 1.5 nm (Figure 3b) or more (Figure S8b) do not aggregate at all, indicating that Pt NP stabilization is possible. Turning to the coking resistance, SEM images of samples annealed in a wet (2% H_2O) methane atmosphere for 25 h are shown in Figure 3c,d. Although intensive carbon deposition was observed in pristine Pt NPs, we found that only a 1.0 nm thick Al_2O_3 layer (Figure S8) can significantly prohibit carbon deposition.

Figure 3e shows the size distribution of Pt particles before and after the heat treatment. It is clear that the Al_2O_3-coated particles retain their original structures, whereas severe agglomeration occurs for the bare Pt. The Fourier transform infrared (FTIR) analysis once again confirms the role of the Al_2O_3 ALD layer in coking inhibition, as shown in Figure 3f. Intense absorption peaks at around 1300 cm^{-1} associated with amorphous carbon and such peaks around 1500 cm^{-1} related to graphitic sp^2 carbon owing to the formation of coked carbon are observed for a bare Pt sample upon exposure to wet (2% H_2O) methane for 25 h. In contrast, the Al_2O_3-coated sample shows dramatically reduced intensity given its lower wavenumber peak, indicating the inhibition of the formation of amorphous carbon on the Pt nanocatalysts.[53] It was reported that the depositions of graphitic carbon and amorphous carbon are the key reasons for the degradation of the catalytic activity because of the blocking of the active sites or the inhibition of the gas accessibility.[54,55] Thus, it can be concluded that the suppressed carbon deposits in this study were mainly due to the greatly reduced amorphous carbon species. Indeed, a coating layer of 1.5 nm or more is necessary to suppress both the agglomeration of Pt particles and carbon coking effectively.

The main reason for the inhibition of coking is the size effect, even if the overcoat layer is gas permeable to gases. It has been proposed that inert modifiers divide catalysts into small ensembles and break up the periodicity of the surface which prevents coke formation.[56] In fact, the pores formed in the Al_2O_3 film are very small, on the nanoscale, and do not sufficiently promote nucleation for coke formation.[56−60] Furthermore, during the ALD process, precursors are primarily deposited onto low-coordination surface sites on a metal catalyst, known as the active centers for carbon decomposition, so that the Al_2O_3 layer deactivates the coke reaction.[43,57,61,62] Thus, the close interaction between Pt particles and the surrounding Al_2O_3 layer enables the realization of a catalyst with good thermal and chemical durability. To the best of our knowledge, this study is the first report in the field of high-temperature electrochemical cells to focus on the introduction of metal nanocatalysts with durability levels drastically improved through an ultrathin Al_2O_3 coating.

We also elucidated the effects of Pt NP deposition and a subsequent Al_2O_3 coating on the electrochemical performance of electrodes by fabricating symmetric cells and analyzing them using EIS. Figure 4a shows the initial impedance responses of the pristine LSCM, bare Pt, and Al_2O_3/Pt samples after the temperature was increased to 650 °C under wet (2% H_2O) methane conditions. To verify the initial electrode performance before severe degradation, which is possible due to coking, we initially raised the temperature in a wet H_2 atmosphere and then started to measure the impedance responses of the samples after quickly changing the gas to wet CH_4. A typical EIS spectrum of a symmetric cell with LSCM electrodes, which is plotted in the Nyquist form, commonly consists of an offset resistance and two semicircles at a lower frequency. The offset resistance is attributed to the YSZ bulk resistance and was omitted from the present spectra to reduce the degree of complexity. Thus, the two impedance arcs reflect the characteristics of the electrochemical reaction occurring on the LSCM electrode. In fact, observations of the electrode impedance spectra, composed of two semicircles, and the corresponding absolute electrode resistance values are shown to be in good agreement with those reported previously by Irvine et al.[10,63] It is beyond the scope of this study to elucidate the detailed origins of the impedance responses of the LSCM electrode; therefore, here, we focused on the sum of the resistances of the two semicircles and used its reciprocal as a factor to represent the electrode activity, where activity is defined here as 1/electrode resistivity (normalized to the electrolyte projected area).

https://dx.doi.org/10.1021/acsami.9b16410
ACS Appl. Mater. Interfaces 2020, 12, 4405−4413

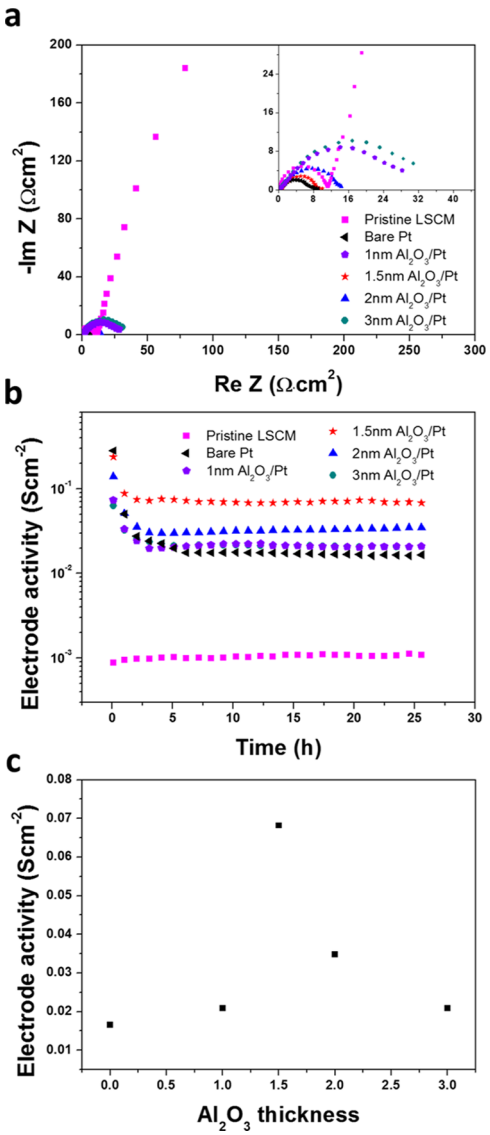

Figure 4. Electrochemical reactivity of Pt-decorated $La_{0.75}Sr_{0.25}Cr_{0.5}Mn_{0.5}O_3$ depending on the thickness of Al_2O_3. (a) Initially measured impedance spectra of pristine LSCM, bare Pt, and Al_2O_3/Pt anode on both sides of a yttria-stabilized ZrO_2 single-crystal electrolyte substrate immediately after elevating the temperature to 650 °C under wet (2% H_2O) CH_4, and (b) stability outcomes of pristine $La_{0.75}Sr_{0.25}Cr_{0.5}Mn_{0.5}O_3$, bare Pt, and Al_2O_3/Pt anodes under identical conditions. (c) Results of the electrode activity depending on the thickness of an overcoat after measuring short-term stability.

The electrode activity of a bare LSCM electrode is considerably large, at about 10^{-3} S·cm^{-2}, because of the insufficient catalytic reactivity of LSCM at a relatively low measurement temperature of 650 °C. In contrast, the deposition of Pt NPs immediately enhances the electrode activity by more than 300 times. These results demonstrate that Pt particles are highly reactive for electrochemical methane oxidation and that the use of Pt NPs is critical when attempting to lower the operating temperature of a SOFC. The electrodes coated with Al_2O_3 on Pt particles also show remarkable performance compared to the bare LSCM. Interestingly, when the thickness of the Al_2O_3 overcoat is 1.5 nm, the highest electrode activity is found, similar to that of Pt particles alone, despite the fact that nearly 80% of the electrode surface is covered by an insulator (Table S3). These observations are consistent with the fact that the Pt NPs aggregate and deteriorate because of coking even in the short time of the heating up and stabilization of the gas atmosphere. It appears that the 1.0 nm protective layer is too thin to stabilize the Pt NPs sufficiently, while 3.0 nm is too thick to allow facile gas accessibility and/or surface reactions. For example, the Al_2O_3 overcoat with a thickness of 3.0 nm passivates nearly 90% of the LSCM surface. This trade-off between protection and reactivity eventually leads to the ideal electrode performance with a 1.5 nm thick Al_2O_3 overcoat. Turning to the time evolution for the performance of the Pt- and Pt/Al_2O_3-decorated electrodes, the Al_2O_3 overcoat is determined to stabilize the electrode, while the activity of the electrode with the bare Pt NPs decreased sharply within 5 h. Figure 4b shows the change in the electrode activity of each sample over time in the wet (2% H_2O) CH_4 atmosphere at 650 °C. All samples except for the pristine LSCM, which underwent high-temperature sintering, show degraded performance levels during longer operating times up to 25 h. However, the electrode coated with 1.5 nm thick Al_2O_3 is rendered highly stable by increasing the resistance by a factor of approximately 3, whereas the performances of electrodes with no Al_2O_3 are sharply degraded by more than 17 times. As a result, the highest electrode activity value of 0.07 S·cm^{-2} is attained for the sample with the 1.5 nm Al_2O_3 layer, even comparable to those reported for a bare LSCM under wet (2% H_2O) CH_4 at the significantly higher temperature of 800 °C.[45] This demonstrates the possibility of decreasing the operating temperature by about 150 °C without sacrificing the reactivity of the anode. To summarize the effect of the Al_2O_3 coating on the electrode activity, Figure 4c shows the electrode activity depending on the thickness of the coating layer after annealing at 650 °C for 25 h under wet (2% H_2O) CH_4. It clearly shows that the optimum coating conditions exist due to the trade-off relationship between the stability and surface coverage of Al_2O_3. Here, we want to emphasize that the ability of ALD to control the thickness to sub-nano levels in an extremely uniform manner gives the insulating material new functionalities.

It is notable that the strategy reported in this work is suitable as a practical and scalable manufacturing route for commercial SOFC applications. Both electrodes and catalysts were fabricated through the most commonly used processes in the SOFC field, and only an ALD process that is commercially available in the semiconductor business was added. ALD does not require a high-temperature heat treatment or an UHV, and the deposition rate is very fast (e.g., the deposition time of the 1.5 nm thick Al_2O_3 was only about 4 min). Furthermore, this strategy is not limited to certain materials and can readily be applied to electrodes, catalysts, and coating layers with various compositions. Therefore, it is possible to implement various functionalities according to the change in the composition and to broaden the application field accordingly. Here, we would like to suggest the following feasible ways to realize higher electrode activities. First, the composition of the coating layer can be replaced with a more conductive and reactive material. The acceptor-doped CeO_2 material can be a good example, as it enables high ionic and electronic conductivity in the atmosphere of interest as well as excellent chemical/electrochemical catalysis properties.[2,64−66] Second, materials more active than LSCM can be used as ceramic electrodes. Electrode materials such as $PrBaMn_2O_5$,[6] $Pr_{0.8}Sr_{1.2}(Co,Fe)_{0.8}Nb_{0.2}O_4$,[67]

https://dx.doi.org/10.1021/acsami.9b16410
ACS Appl. Mater. Interfaces 2020, 12, 4405−4413

and Sr_2MgMoO_6[68] are known to have better electrode activity than LSCM at intermediate temperatures, implying that they can be used to improve overall electrode performance outcomes. Lastly, the electrode activity can be improved by controlling the catalyst compositions and increasing their loading amounts. In this study, we used Pt, the most representative catalyst material, for demonstration purposes, but the literature shows that different precious or alloy-type metals have higher activity levels depending on the fuel type.[69,70] The catalyst loading was fixed in this work, but simply dispersing more catalysts can reduce the electrode resistance even further. Conclusively, given its technical applicability, this work will provide a new perspective to those attempting to realize direct CH_4-fed and low-temperature SOFC electrodes allowing high performance.

CONCLUSIONS

In this study, for the first time, we introduced the ALD of ultrathin films for the stabilization of metal NPs on SOFC anodes to achieve high and stable performance with methane as a fuel. The deposition of Pt NPs onto a LSCM electrode via wet infiltration was determined to enhance the electrode activity dramatically by more than 300 times. However, Pt-decorated electrodes rapidly degrade during the very first stage because of Pt NP agglomeration and carbon deposition. To suppress the electrode degradation, we used Al_2O_3 layers with different thicknesses deposited by ALD. We found that Al_2O_3 layers with thicknesses of 1.0 nm and below cannot efficiently prevent electrode performance degradation. In contrast, when the thickness of the coating layer exceeds 2.0 nm, the performance was not enhanced because of the high surface coverage caused by the insulating Al_2O_3 layer, although high stability was achieved. The trade-off relationship between the surface coverage and stability leads to the ideal thickness of approximately 1.5 nm for efficient and stable electrode performance. It was found that the polarization resistance of the 1.5 nm thick Al_2O_3-coated samples at 650 °C is comparable to previously reported activity levels measured at a significantly higher temperature of 800 °C.[45] Consequently, our results demonstrate that securing metal NPs at the electrode surface with an ultrathin layer deposited by ALD can be a novel approach enabling the use of hydrocarbons as a SOFC fuel while enabling the device operation temperature to be reduced.

EXPERIMENTAL SECTION

Cell Fabrication. The calcined LSCM powder was mixed with the ink vehicle (SOFC materials) by ball-milling to form slurry. It was screen-printed onto the both sides of the YSZ substrate (1 cm × 1 cm and 1 mm thick). It was then dried and sintered at 1200 °C for 1 h at a heating rate of 4 °C/min. Pt NPs were deposited by wet infiltration from the ethanolic solution of chloroplatinic acid. As a current collector, a gold paste was brushed and fired at 700 °C for 1 h.

Physical Characterization of the LSCM Electrode. The microstructures of bare, LSCM/Pt, and LSCM/Pt/ALD electrodes were examined by SEM (Hitachi S-4800). The structures of Al_2O_3-covered Pt NPs were analyzed using the aberration-corrected TEM instrument (JEM-ARM200F, Jeol) equipped with an energy dispersive X-ray spectrometer.

Chemical Characterization. The composition and transition-metal oxidation states were analyzed using the in situ XPS instrument (Axis-Supra, Kratos) with the calibration made using the C 1s peak (C−C bond) at 285.0 eV. The temperature of the samples during the measurements was maintained to 650 °C, and the vacuum level was below 10^{-8} mbar.

Electrochemical Analysis. A symmetric cell was used for the AC impedance spectroscopy (ACIS, VSP-300, Biologic). The AC amplitude of 20 mV at a frequency range of 1 mHz to 1 MHz was used. The cells were placed inside a continuous-flow alumina tube into which wet (2% H_2O) CH_4 were delivered via digital mass flow controllers. The total flow rate was kept constant at 100 sccm (standard temperature and pressure), implying a gas velocity of 19.7 cm min^{-1}.

Al_2O_3 Thin-Film Deposition via ALD. An Al_2O_3 capping layer was deposited by ALD onto the LSCM/Pt anode with trimethylaluminum as an Al_2O_3 precursor and diluted water as an oxidant at a substrate temperature of 180 °C. In a typical run, a number of symmetrical cells were placed on a hand-made metal holder in the middle of the reactor. A typical coating cycle followed the sequence: Al precursor dose (0.5 s)—Ar purge (5 s) water dose (1 s)—Ar purge (15 s).

ASSOCIATED CONTENT

Supporting Information

The Supporting Information is available free of charge at https://pubs.acs.org/doi/10.1021/acsami.9b16410.

Method details, element analysis for the sample, ALD growth behavior, XPS results, EIS results, XRD, and calculation of surface coverage and stability of Pt NPs (PDF)

AUTHOR INFORMATION

Corresponding Authors

Jeong Hwan Kim − *Korea Institute of Machinery & Materials, Daejeon, South Korea, and Hanbat National University, Daejeon, South Korea*; Email: jkim@hanbat.ac.kr

Jeung Ku Kang − *Korea Advanced Institute of Science and Technology (KAIST), Daejeon, South Korea*; orcid.org/0000-0003-3409-7544; Email: jeung@kaist.ac.kr

WooChul Jung − *Korea Advanced Institute of Science and Technology (KAIST), Daejeon, South Korea*; orcid.org/0000-0001-5266-3795; Email: wcjung@kaist.ac.kr

Other Authors

Jongsu Seo − *Korea Advanced Institute of Science and Technology (KAIST), Daejeon, South Korea*

Nikolai Tsvetkov − *Korea Advanced Institute of Science and Technology (KAIST), Daejeon, South Korea*

Seung Jin Jeong − *Korea Advanced Institute of Science and Technology (KAIST), Daejeon, South Korea*; orcid.org/0000-0001-6125-6833

Yeongeun Yoo − *Korea Institute of Machinery & Materials, Daejeon, South Korea*

Sanghoon Ji − *Korea Institute of Civil Engineering and Building Technology, Goyang, South Korea*

Complete contact information is available at: https://pubs.acs.org/10.1021/acsami.9b16410

Author Contributions

J.S. and N.T. contributed equally to this work. J.H.K., J.K.K., and W.J. contributed equally to this work.

https://dx.doi.org/10.1021/acsami.9b16410
ACS Appl. Mater. Interfaces 2020, 12, 4405−4413

Notes

The authors declare no competing financial interest.

■ ACKNOWLEDGMENTS

J.S., S.J.J., and W.J. were financially supported by the Nano Material Technology Development Program (NRF-2017M3A7B4049547), Basic Science Research Program (NRF-2019R1A2C2006006), Frontier R&D Program (2011-0031569), and the Hydrogen Energy Innovation Technology Development Program (NRF-2019M3E6A1064523) through the National Research Foundation of Korea (NRF) funded by the Ministry of Science, ICT and Future Planning. N.T. and J.K.K were also mainly supported by the Global Frontier R&D Program on the Center for Hybrid Interface Materials (2013M3A6B1078884) and the National Research Foundation of Korea (2019M3E6A1104196). J.H.K. and Y.Y. were financially supported by Korea Institute of Machinery and Materials (NK218D).

■ REFERENCES

(1) McIntosh, S.; Gorte, R. J. Direct Hydrocarbon Solid Oxide Fuel Cells. *Chem. Rev.* **2004**, *104*, 4845−4866.
(2) Boldrin, P.; Ruiz-Trejo, E.; Mermelstein, J.; Bermúdez Menéndez, J. M.; Ramírez Reina, T.; Brandon, N. P. Strategies for Carbon and Sulfur Tolerant Solid Oxide Fuel Cell Materials, Incorporating Lessons from Heterogeneous Catalysis. *Chem. Rev.* **2016**, *116*, 13633−13684.
(3) Kwak, N. W.; Jeong, S. J.; Seo, H. G.; Lee, S.; Kim, Y.; Kim, J. K.; Byeon, P.; Chung, S.-Y.; Jung, W. In Situ Synthesis of Supported Metal Nanocatalysts through Heterogeneous Doping. *Nat. Commun.* **2018**, *9*, 4829.
(4) Choi, Y.; Brown, E. C.; Haile, S. M.; Jung, W. Electrochemically Modified, Robust Solid Oxide Fuel Cell Anode for Direct-Hydrocarbon Utilization. *Nano Energy* **2016**, *23*, 161−171.
(5) Metlenko, V.; Jung, W.; Bishop, S. R.; Tuller, H. L.; De Souza, R. A. Oxygen Diffusion and Surface Exchange in the Mixed Conducting Oxides $SrTi_{1-y}Fe_yO_{3-\delta}$. *Phys. Chem. Chem. Phys.* **2016**, *18*, 29495−29505.
(6) Sengodan, S.; Choi, S.; Jun, A.; Shin, T. H.; Ju, Y.-W.; Jeong, H. Y.; Shin, J.; Irvine, J. T. S.; Kim, G. Layered Oxygen-deficient Double Perovskite as an Efficient and Stable Anode for Direct Hydrocarbon Solid Oxide Fuel Cells. *Nat. Mater.* **2015**, *14*, 205.
(7) Jung, W.; Gu, K. L.; Choi, Y.; Haile, S. M. Robust Nanostructures with Exceptionally High Electrochemical Reaction Activity for High Temperature Fuel Cell Electrodes. *Energy Environ. Sci.* **2014**, *7*, 1685−1692.
(8) Jung, W.; Dereux, J. O.; Chueh, W. C.; Hao, Y.; Haile, S. M. High Electrode Activity of Nanostructured, Columnar Ceria Films for Solid Oxide Fuel Cells. *Energy Environ. Sci.* **2012**, *5*, 8682−8689.
(9) Tao, S. W.; Irvine, J. T. S.; Kilner, J. A. An Efficient Solid Oxide Fuel Cell Based upon Single-Phase Perovskites. *Adv. Mater.* **2005**, *17*, 1734−1737.
(10) Tao, S.; Irvine, J. T. S. Synthesis and Characterization of $(La_{0.75}Sr_{0.25})Cr_{0.5}Mn_{0.5}O_{3-\delta}$, a Redox-Stable, Efficient Perovskite Anode for SOFCs. *J. Electrochem. Soc.* **2004**, *151*, A252−A259.
(11) Tao, S.; Irvine, J. T. S. A Redox-Stable Efficient Anode for Solid-Oxide Fuel Cells. *Nat. Mater.* **2003**, *2*, 320−323.
(12) Gao, Z.; Mogni, L. V.; Miller, E. C.; Railsback, J. G.; Barnett, S. A. A Perspective on Low-Temperature Solid Oxide Fuel Cells. *Energy Environ. Sci.* **2016**, *9*, 1602−1644.
(13) White, R. J.; Luque, R.; Budarin, V. L.; Clark, J. H.; Macquarrie, D. J. Supported Metal Nanoparticles on Porous Materials. Methods and applications. *Chem. Soc. Rev.* **2009**, *38*, 481−494.
(14) Bell, A. T. The Impact of Nanoscience on Heterogeneous Catalysis. *Science* **2003**, *299*, 1688−1691.
(15) Cargnello, M.; Fornasiero, P.; Gorte, R. J. Opportunities for Tailoring Catalytic Properties through Metal-Support interactions. *Catal. Lett.* **2012**, *142*, 1043−1048.
(16) Lee, S.; Seo, J.; Jung, W. Sintering-Resistant Pt@CeO_2 Nanoparticles for High-Temperature Oxidation Catalysis. *Nanoscale* **2016**, *8*, 10219−10228.
(17) Monai, M.; Montini, T.; Chen, C.; Fonda, E.; Gorte, R. J.; Fornasiero, P. Methane Catalytic Combustion over Hierarchical Pd@CeO_2/Si-Al_2O_3: Effect of the Presence of Water. *ChemCatChem* **2015**, *7*, 2038−2046.
(18) Kim, S.; Lee, S.; Jung, W. Sintering Resistance of Pt@SiO_2 Core-Shell Catalyst. *ChemCatChem* **2019**, *11*, 4653−4659.
(19) Shim, J. H.; Han, G. D.; Choi, H. J.; Kim, Y.; Xu, S.; An, J.; Kim, Y. B.; Graf, T.; Schladt, T. D.; Gür, T. M. Atomic Layer Deposition for Surface Engineering of Solid Oxide Fuel Cell Electrodes. *Int. J. Precis. Eng. Manuf. Green Technol.* **2019**, *6*, 629.
(20) Karimaghaloo, A.; Koo, J.; Kang, H.-S.; Song, S. A.; Shim, J. H.; Lee, M. H. Nanoscale Surface and Interface Engineering of Solid Oxide Fuel Cells by Atomic Layer Deposition. *Int. J. Precis. Eng. Manuf. Green Technol.* **2019**, *6*, 611.
(21) Zhang, B.; Qin, Y. Interface Tailoring of Heterogeneous Catalysts by Atomic Layer Deposition. *ACS Catal.* **2018**, *8*, 10064−10081.
(22) Singh, J. A.; Yang, N.; Bent, S. F. Nanoengineering Heterogeneous Catalysts by Atomic Layer Deposition. *Annu. Rev. Chem. Biomol. Eng.* **2017**, *8*, 41−62.
(23) Gao, Z.; Qin, Y. Design and Properties of Confined Nanocatalysts by Atomic Layer Deposition. *Acc. Chem. Res.* **2017**, *50*, 2309−2316.
(24) Sobel, N.; Hess, C. Nanoscale Structuring of Surfaces by Using Atomic Layer Deposition. *Angew. Chem., Int. Ed.* **2015**, *54*, 15014−15021.
(25) O'Neill, B. J.; Jackson, D. H.; Lee, J.; Canlas, C.; Stair, P. C.; Marshall, C. L.; Elam, J. W.; Kuech, T. F.; Dumesic, J. A.; Huber, G. W. Catalyst Design with Atomic Layer Deposition. *ACS Catal.* **2015**, *5*, 1804−1825.
(26) Lu, J.; Elam, J. W.; Stair, P. C. Synthesis and Stabilization of Supported Metal Catalysts by Atomic Layer Deposition. *Acc. Chem. Res.* **2013**, *46*, 1806−1815.
(27) Marichy, C.; Bechelany, M.; Pinna, N. Atomic Layer Deposition of Nanostructured Materials for Energy and Environmental Applications. *Adv. Mater.* **2012**, *24*, 1017−1032.
(28) Cassir, M.; Ringuedé, A.; Niinistö, L. Input of Atomic Layer Deposition for Solid Oxide Fuel Cell Applications. *J. Mater. Chem.* **2010**, *20*, 8987−8993.
(29) Rahmanipour, M.; Cheng, Y.; Onn, T. M.; Donazzi, A.; Vohs, J. M.; Gorte, R. J. Modification of LSF-YSZ Composite Cathodes by Atomic Layer Deposition. *J. Electrochem. Soc.* **2017**, *164*, F879−F884.
(30) Roeder, J. F.; Zeberoff, A. F.; Van Buskirk, P. C.; Torabi, A.; Barton, J.; Willman, C.; Ghezel-Ayagh, H.; Huang, K. Behavior of $La_{0.6}Sr_{0.4}Co_{0.2}Fe_{0.2}O_{3-\delta}$ Cathode Powders Surface Modified by Atomic Layer Deposition for Solid Oxide Fuel Cells. *ECS Trans.* **2016**, *75*, 195−202.
(31) Yu, W.; Ji, S.; Cho, G. Y.; Noh, S.; Tanveer, W. H.; An, J.; Cha, S. W. Atomic Layer Deposition of Ultrathin Blocking Layer for Low-Temperature Solid Oxide Fuel Cell on Nanoporous Substrate. *J. Vac. Sci. Technol., A* **2015**, *33*, 01A145.
(32) Liu, K.-Y.; Fan, L.; Yu, C.-C.; Su, P.-C. Thermal Stability and Performance Enhancement of Nano-Porous Platinum Cathode in Solid Oxide Fuel Cells by Nanoscale ZrO_2 Capping. *Electrochem. Commun.* **2015**, *56*, 65−69.
(33) Gong, Y.; Patel, R. L.; Liang, X.; Palacio, D.; Song, X.; Goodenough, J. B.; Huang, K. Atomic Layer Deposition Functionalized composite SOFC cathode $La_{0.6}Sr_{0.4}Fe_{0.8}Co_{0.2}O_{3-\delta}$-$Gd_{0.2}Ce_{0.8}O_{1.9}$: Enhanced Long-Term Stability. *Chem. Mater.* **2013**, *25*, 4224−4231.
(34) Gong, Y.; Palacio, D.; Song, X.; Patel, R. L.; Liang, X.; Zhao, X.; Goodenough, J. B.; Huang, K. Stabilizing Nanostructured Solid Oxide

https://dx.doi.org/10.1021/acsami.9b16410
ACS Appl. Mater. Interfaces 2020, 12, 4405−4413

Fuel Cell Cathode with Atomic Layer Deposition. *Nano Lett.* **2013**, *13*, 4340−4345.
(35) Brahim, C.; Ringuedé, A.; Cassir, M.; Putkonen, M.; Niinistö, L. Synthesis and Properties of ZrO_2-In_2O_3 Overlayers by ALD on the Porous SOFC State-of-the Art Cathode. *ECS Trans.* **2007**, *3*, 261−269.
(36) Ji, S.; Cho, G. Y.; Yu, W.; Su, P.-C.; Lee, M. H.; Cha, S. W. Plasma-Enhanced Atomic Layer Deposition of Nanoscale Yttria-Stabilized Zirconia Electrolyte for Solid Oxide Fuel Cells with Porous Substrate. *ACS Appl. Mater. Interfaces* **2015**, *7*, 2998−3002.
(37) Jang, D. Y.; Kim, H. K.; Kim, J. W.; Bae, K.; Schlupp, M. V. F.; Park, S. W.; Prestat, M.; Shim, J. H. Low-Temperature Performance of Yttria-Stabilized Zirconia Prepared by Atomic Layer Deposition. *J. Power Sources* **2015**, *274*, 611−618.
(38) Ha, S.; Su, P.-C.; Cha, S.-W. Combinatorial Deposition of a Dense Nano-Thin Film YSZ Electrolyte for Low Temperature Solid Oxide Fuel Cells. *J. Mater. Chem. A* **2013**, *1*, 9645−9649.
(39) Brahim, C.; Chauveau, F.; Ringuedé, A.; Cassir, M.; Putkonen, M.; Niinistö, L. ZrO_2−In_2 O_3 Thin Layers with Gradual Ionic to Electronic Composition Synthesized by Atomic Layer Deposition for SOFC Applications. *J. Mater. Chem.* **2009**, *19*, 760−766.
(40) Gourba, E.; Ringuedé, A.; Cassir, M.; Billard, A.; Päiväsaari, J.; Niinistö, J.; Putkonen, M.; Niinistö, L. Characterisation of thin films of ceria-based electrolytes for IntermediateTemperature - Solid oxide fuel cells (IT-SOFC). *Ionics* **2003**, *9*, 15−20.
(41) Choi, H. J.; Bae, K.; Grieshammer, S.; Han, G. D.; Park, S. W.; Kim, J. W.; Jang, D. Y.; Koo, J.; Son, J.-W.; Martin, M.; Shim, J. H. Surface Tuning of Solid Oxide Fuel Cell Cathode by Atomic Layer Deposition. *Adv. Energy Mater.* **2018**, *8*, 1802506.
(42) Shim, J. H.; Jiang, X.; Bent, S. F.; Prinz, F. B. Catalysts with Pt Surface Coating by Atomic Layer Deposition for Solid Oxide Fuel Cells. *J. Electrochem. Soc.* **2010**, *157*, B793−B797.
(43) Lu, J.; Fu, B.; Kung, M. C.; Xiao, G.; Elam, J. W.; Kung, H. H.; Stair, P. C. Coking-and Sintering-Resistant Palladium Catalysts Achieved through Atomic Layer Deposition. *Science* **2012**, *335*, 1205−1208.
(44) Kim, Y.; Jeong, S. J.; Koo, B.; Lee, S.; Kwak, N. W.; Jung, W. Study of the Surface Reaction Kinetics of (La,Sr)$MnO_{3-\delta}$ Oxygen Carriers for Solar Thermochemical Fuel Production. *J. Mater. Chem. A* **2018**, *6*, 13082−13089.
(45) Jiang, S.; Chen, X.; Chan, S.; Kwok, J.; Khor, K. $La_{0.75}Sr_{0.25}$)-$(Cr_{0.5}Mn_{0.5})O_3$/YSZ Composite Anodes for Methane Oxidation Reaction in Solid Oxide Fuel Cells. *Solid State Ionics* **2006**, *177*, 149−157.
(46) Nur, A. S. M.; Funada, E.; Kiritoshi, S.; Matsumoto, A.; Kakei, R.; Hinokuma, S.; Yoshida, H.; Machida, M. Phase-Dependent Formation of Coherent Interface Structure between PtO_2 and TiO_2 and Its Impact on Thermal Decomposition Behavior. *J. Phys. Chem. C* **2018**, *122*, 662−669.
(47) Vinayan, B. P.; Ramaprabhu, S. Platinum−TM (TM= Fe, Co) Alloy Nanoparticles Dispersed Nitrogen Doped (Reduced Graphene Oxide-Multiwalled Carbon Nanotube) Hybrid Structure Cathode Electrocatalysts for High Performance PEMFC Applications. *Nanoscale* **2013**, *5*, 5109−5118.
(48) Vovk, E. I.; Kalinkin, A. V.; Smirnov, M. Y.; Klembovskii, I. O.; Bukhtiyarov, V. I. XPS Study of Stability and Reactivity of Oxidized Pt Nanoparticles Supported on TiO_2. *J. Phys. Chem. C* **2017**, *121*, 17297−17304.
(49) Toda, T.; Igarashi, H.; Uchida, H.; Watanabe, M. Enhancement of the Electroreduction of Oxygen on Pt Alloys with Fe, Ni, and Co. *J. Electrochem. Soc.* **1999**, *146*, 3750−3756.
(50) Ponce, S.; Peña, M. A.; Fierro, J. L. G. Surface Properties and Catalytic Performance in Methane Combustion of Sr-Substituted Lanthanum Manganites. *Appl. Catal., B* **2000**, *24*, 193−205.
(51) Tao, S.; Irvine, J. T. S.; Plint, S. M. Methane Oxidation at Redox Stable Fuel Cell Electrode $La_{0.75}Sr_{0.25}Cr_{0.5}Mn_{0.5}O_{3-\delta}$. *J. Phys. Chem. B* **2006**, *110*, 21771−21776.
(52) Cheng, X.; Li, Y.; Zheng, L.; Yan, Y.; Zhang, Y.; Chen, G.; Sun, S.; Zhang, J. Highly Active, Stable Oxidized Platinum Clusters as Electrocatalysts for the Hydrogen Evolution Reaction. *Energy Environ. Sci.* **2017**, *10*, 2450−2458.
(53) Smith, B. C. *Infrared Spectral Interpretation: A Systematic Approach*; CRC Press, 1998.
(54) Al-Fatesh, A. S.; Arafat, Y.; Atia, H.; Ibrahim, A. A.; Ha, Q. L. M.; Schneider, M.; M-Pohl, M.; Fakeeha, A. H. CO_2-Reforming of Methane to Produce Syngas Over Co-Ni/SBA-15 Catalyst: Effect of Support Modifiers (Mg, La and Sc) on Catalytic Stability. *J. CO_2 Util.* **2017**, *21*, 395−404.
(55) Guo, J.; Lou, H.; Zheng, X. The Deposition of Coke From Methane on a Ni/$MgAl_2O_4$ Catalyst. *Carbon* **2007**, *45*, 1314−1321.
(56) Han, J. W.; Kim, C.; Park, J. S.; Lee, H. Highly Coke-Resistant Ni Nanoparticle Catalysts with Minimal Sintering in Dry Reforming of Methane. *ChemSusChem* **2014**, *7*, 451−456.
(57) Lu, J.; Liu, B.; Greeley, J. P.; Feng, Z.; Libera, J. A.; Lei, Y.; Bedzyk, M. J.; Stair, P. C.; Elam, J. W. Porous Alumina Protective Coatings on Palladium Nanoparticles by Self-Poisoned Atomic Layer Deposition. *Chem. Mater.* **2012**, *24*, 2047−2055.
(58) Nikolla, E.; Schwank, J.; Linic, S. Comparative Study of the Kinetics of Methane Steam Reforming on Supported Ni and Sn/Ni alloy Catalysts: the Impact of the Formation of Ni Alloy on Chemistry. *J. Catal.* **2009**, *263*, 220−227.
(59) Nikolla, E.; Schwank, J.; Linic, S. Promotion of the Long-Term Stability of Reforming Ni Catalysts by Surface Alloying. *J. Catal.* **2007**, *250*, 85−93.
(60) Nikolla, E.; Holewinski, A.; Schwank, J.; Linic, S. Controlling Carbon Surface Chemistry by Alloying: Carbon Tolerant Reforming Catalyst. *J. Am. Chem. Soc.* **2006**, *128*, 11354−11355.
(61) Rovik, A. K.; Klitgaard, S. K.; Dahl, S.; Christensen, C. H.; Chorkendorff, I. Effect of Alloying on Carbon Formation during Ethane Dehydrogenation. *Appl. Catal., A* **2009**, *358*, 269−278.
(62) Liu, Z.-P.; Hu, P. General Rules for Predicting Where a Catalytic Reaction Should Occur on Metal Surfaces: A Density Functional Theory Study of C−H and C−O Bond Breaking/Making on Flat, Stepped, and Kinked Metal Surfaces. *J. Am. Chem. Soc.* **2003**, *125*, 1958−1967.
(63) Primdahl, S.; Mogensen, M. Gas Diffusion Impedance in Characterization of Solid Oxide Fuel Cell Anodes. *J. Electrochem. Soc.* **1999**, *146*, 2827−2833.
(64) Choi, Y.; Cha, S. K.; Ha, H.; Lee, S.; Seo, H. K.; Lee, J. Y.; Kim, H. Y.; Kim, S. O.; Jung, W. Unravelling Inherent Electrocatalysis of Mixed-Conducting Oxide Activated by Metal Nanoparticle for Fuel Cell Electrodes. *Nat. Nanotechnol.* **2019**, *14*, 245.
(65) Oh, T.-S.; Tokpanov, Y. S.; Hao, Y.; Jung, W.; Haile, S. M. Determination of Optical and Microstructural Parameters of Ceria Films. *J. Appl. Phys.* **2012**, *112*, 103535.
(66) Ling, Y.; Xie, H.; Liu, Z.; Du, X.; Chen, H.; Ou, X.; Zhao, L.; Budiman, R. A. Enhanced Electrochemical Activity and Chromium Tolerance of the Nucleation-Agent-Free $La_2Ni_{0.9}Fe_{0.1}O_{4+\delta}$ Cathode by $Gd_{0.1}Ce_{0.9}O_{1.95}$ Incorporation. *Electron. Mater. Lett.* **2018**, *14*, 432−439.
(67) Yang, C.; Yang, Z.; Jin, C.; Xiao, G.; Chen, F.; Han, M. Sulfur-Tolerant Redox-Reversible Anode Material for Direct Hydrocarbon Solid Oxide Fuel Cells. *Adv. Mater.* **2012**, *24*, 1439−1443.
(68) Huang, Y.-H.; Dass, R. I.; Xing, Z.-L.; Goodenough, J. B. Double Perovskites as Anode Materials for Solid-Oxide Fuel Cells. *Science* **2006**, *312*, 254−257.
(69) Thompson, S. T.; Papageorgopoulos, D. Platinum Group Metal-Free Catalysts Boost Cost Competitiveness of Fuel Cell Vehicles. *Nat. Catal.* **2019**, *2*, 558−561.
(70) Morozan, A.; Jousselme, B.; Palacin, S. Low-Platinum and Platinum-Free Catalysts for the Oxygen Reduction Reaction at Fuel Cell Cathodes. *Energy Environ. Sci.* **2011**, *4*, 1238−1254.

https://dx.doi.org/10.1021/acsami.9b16410
ACS Appl. Mater. Interfaces 2020, 12, 4405−4413